Journal of Materials Chemistry B

ROYAL SOCIETY OF CHEMISTRY

PAPER

View Article Online
View Journal

Cite this: DOI: 10.1039/d3tb00125c

Dual-targeted poly(amino acid) nanoparticles deliver drug combinations on-site: an intracellular synergistic strategy to eliminate intracellular bacteria†

Dongdong Zhao,[a] Wenli Feng,[a] Xiaoxu Kang,[a] Haofei Li,[a] Fang Liu,[b] Weitao Zheng,[c] Guofeng Li*[a] and Xing Wang *[a]

Multi-drug combinations are a common strategy for the treatment of intracellular bacterial infections. However, different internalized pathways and the accumulation of the composite drugs at different subcellular organelles very much reduce their efficacy. Herein, an intracellular synergistic strategy is proposed, which is realized by on-site delivery of a drug combination using a macrophage/intracellular bacterium-dual targeted drug delivery system (DDS). The DDS is fabricated by encapsulating vancomycin (Van) and curcumin (Cur) into poly(α-*N*-acryloyl-phenylalanine)-*block*-poly(β-*N*-acryloyl-D-amino-alanine-*co*-2-*O*-acetyl-α-D-mannosyloxy) nanoparticles, denoted by (Van + Cur)@F(AM) NPs. Mannose ligands on (Van + Cur)@F(AM) NPs trigger their specific internalization in macrophages, while aminoalanine moieties subsequently drive the NPs to target intracellular methicillin-resistant *Staphylococcus aureus* (MRSA). Thereafter, Van and Cur are durably released in a synergistic dose at the residence site of intracellular MRSA. Under this intracellular synergistic effect, (Van + Cur)@F(AM) NPs show superior elimination efficiency *in vitro* and *in vivo* compared to the control groups, including free Van, (Van + Cur), the DDS encapsulated Van and the DDSs separately-encapsulated Van and Cur. Furthermore, (Van + Cur)@F(AM) NPs significantly enhance the *in vivo* antibacterial capacity by modulating the immune response. Therefore, this dual-targeted DDS-assisted intracellular synergistic antibacterial strategy of drug combination is an effective therapeutic against intracellular bacteria.

Received 20th January 2023,
Accepted 2nd March 2023

DOI: 10.1039/d3tb00125c

rsc.li/materials-b

1 Introduction

Recurrent infections caused by intracellular bacteria have long been a difficult problem for human public health.[1] Bacteria persist in cells and induce latent infections that lead to diseases including osteomyelitis, sepsis, and necrotizing pneumonia.[2] Usually, treatment requires long-term and continuous drug action. Unfortunately, treatment failure and relapse are common.[3–5] Professional phagocytes are the first line of defense against bacterial infections, which work by recognizing, ingesting, and digesting invasive pathogens,[6,7] but intracellular bacteria are difficult to eliminate because they can evade the immune response and survive even when engulfed by phagocytes.[7] In this case, phagocytes not only fail to eradicate the bacteria but also become a source of bacterial multiplication and thus cause predisposition to recurrent infections.[8,9] In addition, because of intracellular penetration and accumulation of many conventional antibiotics, more than two-thirds of prescribed antibiotics are ineffective and cause severe systemic toxicity.[10,11] Therefore, the eradication of intracellular bacteria is a challenging task for clinical medicine.

To improve treatment outcomes, the advantages of combination therapy have been gaining prominence in recent years.[12–15] It has been reported that the co-administration of conventional antibiotics with other antibiotics or non-antibiotic drugs may improve treatment efficiency compared to the effectiveness of individual antibiotic therapy.[16–20] Moreover, combination therapy can effectively reduce the therapeutic dose and possible side effects compared to the original individual drugs.[21] Vancomycin (Van) is a classical first-line drug and is often seen as a last resort,[22–25] but Van alone has limited therapeutic

[a] State Key Laboratory of Organic–Inorganic Composites, Beijing Laboratory of Biomedical Materials, Beijing University of Chemical Technology, Beijing 100029, P. R. China. E-mail: ligf@mail.buct.edu.cn, wangxing@mail.buct.edu.cn
[b] Department of Oncology of Integrative Chinese and Western Medicine, China-Japan Friendship Hospital, Beijing, 100029, China
[c] Hubei Provincial Key Laboratory of Industrial Microbiology, Sino-German Biomedical Center, National "111" Center for Cellular Regulation and Molecular Pharmaceutics, Hubei University of Technology, Wuhan, 430068, Hubei Province, China

† Electronic supplementary information (ESI) available. See DOI: https://doi.org/10.1039/d3tb00125c

efficacy for intracellular bacterial infections.[26] Therefore, choosing a suitable drug in combination with Van is expected to improve the therapeutic effect of Van. Curcumin (Cur) is a natural compound derived from turmeric.[27–29] Recent studies showed the potential of Cur for reversing the bacterial resistance to Van.[30] In addition, Cur has been shown to have anti-inflammatory activity and can induce immunity in the body.[31] Therefore, combining Cur with Van is expected to improve the therapeutic effect of intracellular bacterial infections. However, the interception of host cells is an obstacle to the internalization of the drug combination, and their synergistic bactericidal properties cannot be exerted in this situation. The main reasons are: (i) different internalized pathways of the drugs result in different and suboptimal intracellular accumulation;[32] (ii) drugs in the combined formulation will stay at different subcellular organelles because of their inherent characteristics;[32] (iii) the drugs have short residence times owing to the efflux effect of the host cells;[33] (iv) the bactericidal activity of the drugs will be attenuated because of the harsh intracellular microenvironment (*e.g.* acidic pH, enzymes).[34] As such, differences in the intracellular spatio-temporal distribution of the drug combination and interference of the host cells very much reduce the synergistic efficacy of the drug combination against intercellular bacterial infections.

A drug delivery system (DDS) can overcome the cell membrane barrier and has great advantages in the treatment of intracellular infections.[35–39] For instance, Nataša Škalko-Basnet designed a liposomal vesicle that effectively increases antibiotic accumulation in host cells.[40] Zhang and co-workers proposed a bacteria-responsive biomimetic polymeric nanoplatform that directly releases clarithromycin at the location of intracellular bacteria.[41] Recently, we developed poly(amino acid)-based DDSs,[42,43] which effectively deliver antibiotics at the location of intracellular bacteria *via* macrophages and bacteria cascade-targeting.[44] This DDS is able to overcome the interference of the host cells and differences in the intracellular spatiotemporal distribution of the drugs, showing great potential for delivering drug combinations. But it cannot be ignored that premature and differential drug release from the DDS prior to reaching the site of infection alters the formulation of the drug combination, resulting in an attenuated bactericidal efficacy. Besides, the increased bacterial drug resistance caused by a harsh intracellular microenvironment further requires the continuous action of the drug combination over a long period.[45] Therefore, to achieve the synergistic bactericidal performance of the drug combination, two key challenges of the DDS need to be solved: (i) enabling effective dose encapsulation of the drug combination, and (ii) exerting durable synergistic bactericidal effects on-site.

Herein, a robust DDS based on poly(α-*N*-acryloyl-phenylalanine)-*block*-poly(β-*N*-acryloyl-D-aminoalanine-*co*-2-*O*-acetyl-α-D-mannosyloxy) (F(AM)) was fabricated *via* a facile copolymerization technique (Scheme 1). Inspired by, but different from, the previous study,[44] hydrophilic fractions in F(AM) were obtained *via* a typical copolymerization procedure of β-*N*-acryloyl-D-aminoalanine monomer and 2-*O*-acetyl-α-D-mannosyloxy monomer. It was critical to improve the packaging capacity of the cargo and the stability of the DDS, so as to evoke its potential to achieve long-term, sustainable and stable multi-drug release. After optimization, Van and Cur were encapsulated into the F(AM) nanoparticles (NPs) at the preset dose, and the resulting encapsulation was denoted by (Van + Cur)@F(AM) NPs. (Van + Cur)@F(AM) NPs were engulfed by macrophages *via* mannose receptor-mediated internalization, and then specifically targeted to intracellular methicillin-resistant *Staphylococcus aureus* (MRSA) through peptidoglycan anchoring of amino alanine moieties. As such, (Van + Cur)@F(AM) NPs were able to deliver the drug combination on-site, which effectively broke through the multiple physiological barriers described above. Furthermore, Van and Cur in the (Van + Cur)@F(AM) NPs were released in uniform and long-term patterns, facilitating their durable synergistic bactericidal effects. Consequently, (Van + Cur)@F(AM) NPs showed the best *in vitro* and *in vivo* intracellular MRSA elimination effect compared to other controls, including free Van, (Van + Cur), the DDS encapsulated Van and the DDSs separately-encapsulated Van and Cur. In addition, (Van + Cur)@F(AM) NPs could mobilize the body's immunity by modulating immune cytokines, allowing for enhanced therapeutic efficacy against intracellular bacterial infections. Therefore, (Van + Cur)@F(AM) NPs, exerting the intracellular synergistic effect of drug combination *via* on-site delivery, offer great promise in the fight against intracellular bacterial infection.

2 Materials and methods

2.1 Materials

L-Phenylalanine (≥97%), α-Boc-D-aminoalanine (≥98%), mannose (≥98%), acryloyl chloride (≥98%), α-D-mannose pentaacetate (≥97%), 2-hydroxyethyl acrylate (HEA, ≥98%), 2-(dodecylthiocarbonothioylthio)-2-methylpropionic acid (DDMAT, ≥98%), boron (tri) fluoride etherate (BF_3Et_2O, ≥97%), tris[2-phenylpyridinato-C^2,N]iridium(III) ($Ir(ppy)_3$, ≥99%), trimethylsilyldiazomethane ($TMSCHN_2$, *ca.* 10% in hexane, 0.6 mol L^{-1}), Van (≥98%), Cur (≥98%), Nile red (NR, ≥98%), fluorescein isothiocyanate (FITC, ≥97%) and other common solvents such as dimethyl sulfoxide (DMSO), dichloromethane (DCM), ethanol (EtOH), methanol (MeOH), tetrahydrofuran (THF), trifluoroacetic acid (TFA) and ethyl acetate (EA) were purchased from J&K Scientific. Tryptic soy broth (TSB) and tryptose soy agar (TSA) were purchased from Sinopharm Chemical Reagent (China).

Cell culture medium was purchased from Gibco BRL (U.S.A.) and CORNING (U.S.A.). Thiazolyl blue tetrazolium bromide (MTT), Lyso-Tracker Red, calcein AM, diamidine phenyl indole (DAPI), lysostaphin, and Triton X-100 were purchased from Solar Science & Technology Co., Ltd. (China).

2.2 F(AM) synthesis

2.2.1 Synthesis of monomers. The α-*N*-acryloyl-phenylalanine (denoted by F), β-*N*-acryloyl-α-Boc-D-aminoalanine (denoted by A_{Boc}), and 2-(2′,3′,4′,6′-tetra-*O*-acetyl-α-D-mannosyloxy) ethyl acrylate (denoted by M_{OAc}) monomers were

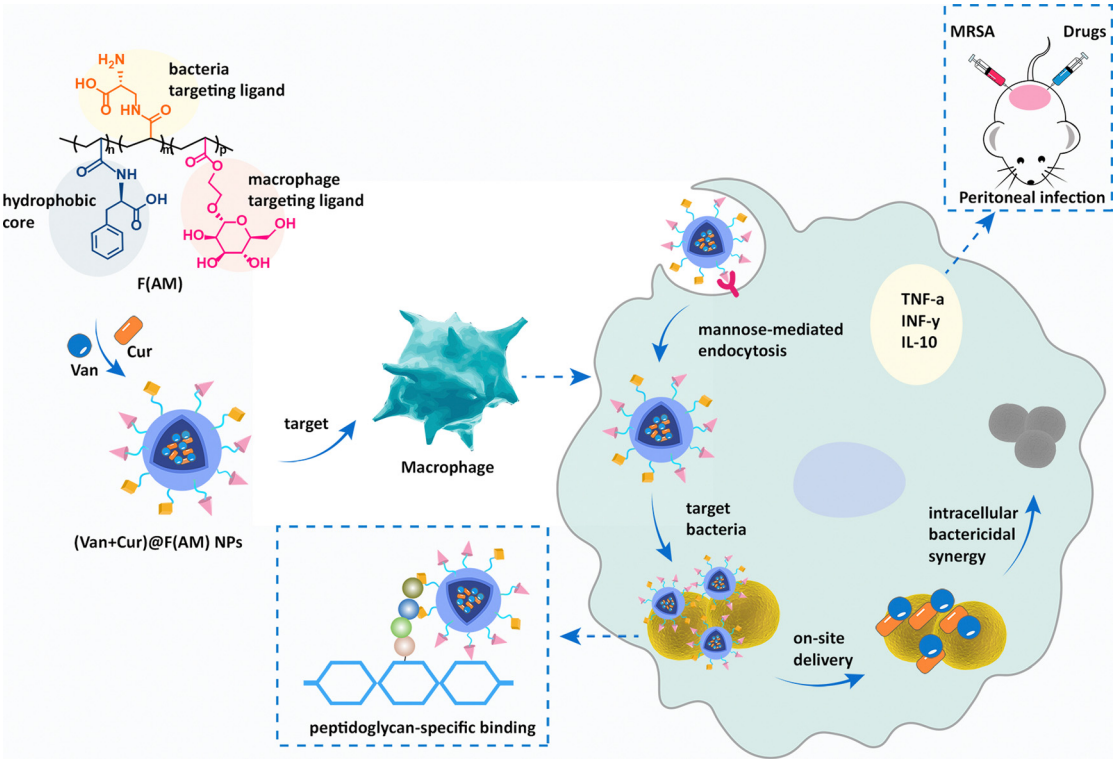

Scheme 1 Schematic diagram of the fabrication and intracellular bacteria elimination of (Van + Cur)@F(AM) NPs. (a) Van and Cur can be successfully encapsulated in the DDS in a preset dose to form (Van + Cur)@F(AM) NPs. (b) (Van + Cur)@F(AM) NPs exert an intracellular synergistic bactericidal effect *via* on-site delivery of the drug combination. Specifically, (Van + Cur)@F(AM) NPs are engulfed by macrophages *via* mannose receptor-mediated internalization, and then specifically target intracellular bacteria through peptidoglycan anchoring of amino alanine moieties. Van and Cur are released on-site and eliminate intracellular bacteria by synergistic action. (Van + Cur)@F(AM)NPs are able to induce an immune response *in vivo*, by modulating immune factors.

synthesized by the previously reported method. They were all successfully synthesized as demonstrated by ^{1}H NMR.[43]

2.2.2 F(AM) synthesis. Poly(α-*N*-acryloyl-phenylalanine) (denoted by PF) was synthesized first using photoinduced electron/energy transfer-reversible addition-breakage chain transfer (PET-RAFT) polymerization.[46] Then, PF was used as the macro-chain transfer agent (CTA) for the synthesis of poly(α-*N*-acryloyl-phenylalanine)-*block*-poly(β-*N*-acryloyl-α-Boc-D-aminoalanine-*co*-2-(2′,3′,4′,6′-tetra-*O*-acetyl-α-D-mannosyloxy) ethyl acrylate) (denoted by $F(A_{Boc}M_{OAc})$). Typically, the monomer A_{Boc} (1 g, 3.87 mmol) or M_{OAc} (1.7 g, 3.87 mmol), PF (0.83 g, 0.129 mmol), and $Ir(ppy)_3$ (25 mg, 3.87×10^{-5} mmol) were dissolved in 1 mL of DMSO. The reaction was then degassed first with N_2 for 30 min followed by irradiation under blue light for 6 h. The polymers were purified according to our previous method.[43]

The newly synthesized $F(A_{Boc}M_{OAc})$ was deprotected by deacetylation as well as by removal of *tert*-butoxy carbonyl protection. First, $F(A_{Boc}M_{OAc})$ (220 mg) and sodium methanol (30 mg) were dissolved in 4 mL of MeOH, stirred using a magnetic stirrer for 4 h, then dialyzed in a MeOH solution for 48 h with a 1000 Da dialysis bag to obtain poly(α-*N*-acryloyl-phenylalanine)-*block*-poly(β-*N*-acryloyl-α-Boc-D-aminoalanine-*co*-2-*O*-acetyl-α-D-mannosyloxy) (denoted by $F(A_{Boc}M)$). The obtained $F(A_{Boc}M)$ (400 mg) was dispersed in a DCM/THF (1 mL/200 μL) mixed solution for 3 h and dialyzed in MeOH solution with 1000 Da for 48 h. The F(AM) was collected and dried.

2.3 Preparation of delivery systems

For $(Van_{1.5} + Cur_{3.0})$@F(AM) NPs, F(AM) copolymer (10 mg), Van (2.5 mg), and Cur (5.5 mg) were dissolved in 1 mL of DMSO, and then 9 mL of distilled water was added under high-speed stirring (>1000 rpm), with agitation for 30 min, following by dialysis with ultrapure water for 48 h. Similar methods were used to prepare Van@F(AM) NPs, and Cur@F(AM) NPs. DLS and TEM were used to evaluate the size, zeta potential, morphology, and stability of the NPs.

2.4 Drug loading rate (DLC), and encapsulation rate (DLE)

The DLC (%) and DLE (%) of Van and Cur were calculated by the following equations.

$$\text{DLC (\%)} = (\text{weight of drug load/total weight of polymer and load drug}) \times 100\%$$

$$\text{DLE (\%)} = (\text{weight of drug load/total weight of drug}) \times 100\%$$

2.4.1 Drug release. (Van + Cur)@F(AM) NPs were dispersed in PBS solution at pH 7.4. They were then placed in dialysis

bags (MWCO 3500 Da) and immersed in 5 mL of PBS buffer containing 0.5% w/v Twain 80. The dialysis system was incubated on a 37 °C shaker, and 1 mL of the solvent outside the dialysis bag was removed periodically and supplemented with 1 mL of PBS buffer containing 0.5% w/v Twain 80. The release of Cur and Van was analyzed by UV-Vis and HPLC, respectively.

2.5 On-site delivery

2.5.1 Targeting cells. Rat fibroblast cells L929 and murine macrophages RAW264.7 were inoculated separately in confocal culture dishes at 2×10^5 mL^{-1} cells per dish and incubated overnight. RAW264.7 macrophages were labeled with calcein AM, mixed with L929 fibroblasts (unlabeled) at a 1:1 ratio, and cultured in a 1:1 medium mixture. Co-cultured cells were treated with Nile Red-loaded F(AM) NPs (denoted by NR@F(AM) NPs, 10 μg mL^{-1} NR) for 1 h and washed three times with PBS. Cells were then fixed in 4% paraformaldehyde (20 min). Finally, cells were stained with diamidine phenyl indole (DAPI) (5–10 min) and observed using a confocal laser scanning microscope (CLSM).

2.5.2 Targeting bacteria. Exponentially grown MRSA was incubated with FITC (5 μg mL^{-1}) in saline at 37 °C for 2 h to form FITC-MRSA. Then RAW264.7 macrophages were washed three times with PBS and then infected with FITC-MRSA followed by co-culture with NR@F(AM) NPs (10 μg mL^{-1} NR) for 24 h after infection. The RAW264.7 macrophages were fixed with 4% paraformaldehyde for 20 min, then stained with DAPI for 5-10 min and imaged using CLSM.

2.6 Extracellular antibacterial evaluation

2.6.1 Bacterial culture. MRSA (MRSA-1857) used in this study was isolated from the Affiliated Hospital of the Chinese Academy of Military Medical Sciences. MRSA was incubated in a TSB medium at 37 °C for 9 h. Subsequently, the suspension was centrifuged at 3500 rpm for 3 min to collect MRSA and washed twice with saline.

2.6.2 Minimum inhibition concentration (MIC). The MIC was determined by serial dilution of compounds in 96-well plates containing broth medium (100 μL). In brief, broth medium (100 μL) containing two-fold serial dilutions of each compound was placed in a 96-well plate. Briefly, MRSA strains were collected in the cultures during the exponential growth period, diluted to 5×10^6 CFU mL^{-1}, and inoculated in 96-well plates. The MIC was determined by incubation at 37 °C for 24 h. The final MIC was determined from the optical density (OD) value at 600 nm. The MIC is the concentration corresponding to the wells in which no MRSA growth is observed. The broth containing MRSA was used as a positive control and the broth without MRSA as a negative control. Each test was repeated three times.

2.6.3 Checkerboard method. The fractional inhibition concentration index (FICI) was measured. The synergistic effect between Van and Cur was evaluated by the checkerboard method. Van and Cur were mixed in a 96-well plate in serial two-dimensional dilutions. The bacteria were then similarly inoculated in 96-well plates and OD_{600} values were measured. The FICI was calculated according to the following formula to assess the synergy effect.

$$\mathrm{FICI} = \frac{\mathrm{MICA\ in\ combination}}{\mathrm{MICA}} + \frac{\mathrm{MICB\ in\ combination}}{\mathrm{MICB}}$$

The FICI data were interpreted as follows: complete synergy when FICI $\leq$ 0.5, partial synergy when 0.5 $<$ FICI $\leq$ 0.75, ineffective when 0.75 $<$ FICI $\leq$ 2, or antagonistic antibacterial performance evaluation when FICI $>$ 2.[47]

2.6.4 Extracellular bacterial colony count. MRSA was co-incubated with different concentrations of drugs at 37 °C for 24 h and then diluted and spread onto TSA agar plates in triplicate and incubated for 24 h, followed by counting of bacterial colonies.

2.7. Intracellular antibacterial evaluation

2.7.1. Cell culture. RAW264.7 macrophages were cultured by incubating with Dulbecco's modified eagle's medium (DMEM) supplemented with 10% fetal bovine serum (FBS) and 1% antibiotic and antifungal solutions (penicillin and streptomycin) at 37 °C and 5% CO_2 in an incubator, and the medium was changed every other day.

2.7.2. Construction of intracellular bacteria. RAW264.7 macrophages were plated at 50 000 cells per well and incubated for 18–24 h. The MRSA was inoculated at 25 times the number of cells per well. After infecting for 1 h, the RAW264.7 macrophages were washed three times with PBS. Then, gentamicin was added at 50 μg mL^{-1} per well (1 mL) and incubated for 1 h to kill extracellular MRSA.

2.7.3. Intracellular antibacterial evaluation. First, RAW264.7 macrophages infected with MRSA were washed three times with PBS, and then incubated with Van, Van + Cur, Van@FAM NPs, Van@FAM NPs + Cur@FAM NPs, and (Van + Cur)@FAM NPs for 12, 24, and 48 h. Finally, RAW264.7 macrophages were lysed with PBS containing 0.1% (v/v) Triton X-100. After lysis, the obtained intracellular MRSA was diluted and spread in triplicate onto TSA agar plates. MRSA was incubated overnight and then counted against the colony count.

2.7.4. Cellular uptake of the NPs. RAW264.7 macrophages were inoculated in confocal culture dishes (3×10^5 mL^{-1}) for CLSM. NR@F(AM) NPs (10 μg mL^{-1} NR) were added to the culture medium. After co-incubation at different times, RAW264.7 macrophages were observed using CLSM. The mean fluorescence intensity (MFI) was analyzed by the software Image J.

2.7.5. Cellular internalization mechanisms. The cellular internalization mechanism of the NPs was analyzed using internalization inhibitors. In brief, RAW264.7 macrophages were spread flat into confocal culture dishes (3×10^5 mL^{-1}) and incubated for 24 h. The cells were separately pretreated with methyl-β-cyclodextrin (β-CD, 5 mM), amiloride (2 mM), chlorpromazine (chlorpromazine hydrochloride, 10 μg mL^{-1}), and sucrose (450 mM) for 1 h. The control group was pretreated with PBS only. After pretreatment, FITC@F(AM) NPs were added to each well (5 μg mL^{-1} FITC) and incubated for another

4 h. Then, the treated RAW264.7 macrophages were observed with CLSM. Relative endocytosis was analyzed by the software Image J.

2.7.6. Mannose-mediated competitive inhibition of uptake. RAW264.7 macrophages were spread flat into confocal culture dishes (3×10^5 mL^{-1}) and incubated for 24 h. They were pretreated with 25 mM and 50 mM mannose as well as PBS for 1 h. FITC@F(AM) NPs (5 μg mL^{-1} FITC) were added and incubated for 3 h. Then, the treated RAW264.7 macrophages were observed with CLSM.

2.7.7. Lysosomal escape. RAW264.7 macrophages were inoculated in confocal culture dishes (3×10^5 mL^{-1}) and incubated for 24 h, then incubated with Lyso-Tracker red for 1 h. After further incubation with FITC@F(AM) NPs (5 μg mL^{-1} FITC) at different times, the cells were washed with PBS and imaged with CLSM.

2.8. *In vivo* antibacterial effect

2.8.1. Mice handling. Balb/c female mice (6–7 weeks) were purchased from Beijing Charles River Co., Ltd. In this study, all animal care was in accordance with the National Research Council Guide for the Care and Use of Laboratory Animals. All animal experiments were supervised and evaluated under the supervision and evaluation of the SPF Animal Section of the Clinical Research Institute of China-Japan Friendship Hospital (Approval no. zryhyy 12-20-08-3).

2.8.2. *In vivo* antibacterial activity (peritonitis model). The MRSA-infected peritonitis model was used to evaluate the antibacterial effect *in vivo*. Briefly, mice were injected intraperitoneally (i.p.) with MRSA (2×10^8 CFU per mouse, 100 μL) for 24 h. Then, the mice were randomized into 3 groups ($n = 3$) and treated in different groups for 24 h by injecting with a single dose (i.p.) of PBS, (Van + Cur), or (Van + Cur)@F(AM) (10 mg kg^{-1} Van; 20 mg kg^{-1} Cur). Finally, the mice were euthanized and injected (i.p.) with 2 mL of HBSS. Peritoneal fluid was collected to determine the total, extracellular and intracellular CFU. The peritoneal fluid was combined with hemolysin (15 μg mL^{-1}) to kill extracellular MRSA and lysed with HBSS containing 0.1% Triton X to quantify intracellular CFU. Blood was drawn from the orbital sinus to detect pro-inflammatory markers in the serum. Major organs were collected. The liver, spleen, lungs, and kidneys were evaluated with hematoxylin and eosin (H&E).

2.9. Biological activity

2.9.1. Cytotoxicity assay. RAW264.7 macrophages and L929 fibroblasts were used for the MTT assay. Cells were inoculated onto 96-well plates (5000 cells per well) and incubated at 37 °C with 5% CO_2 in an incubator for 24 h to adhere them to the wall. Then (Van + Cur)@F(AM) NPs were added to each well with serial dilutions. After 24 h of incubation, 10 μL of 5 mg mL^{-1} MTT solution was added to each well and they were incubated for another 4 h at 37 °C. Finally, the mixture was removed. 100 μL of 10% SDS was added, and the absorbance was measured at 570 nm.

2.9.2. Hemolysis. Fresh mouse blood samples were collected by centrifugation at 5000 rpm (5 min). Blood cells were washed three times with PBS after a final concentration of approximately 5% (v/v). (Van + Cur)@F(AM) NPs were serially diluted with PBS and placed simultaneously with the same volume of blood cell suspension in a 96-well plate and incubated at 37 °C for 4 h. After that, the suspension was collected and centrifuged at 3000 rpm (7 min) and the supernatant was collected to monitor the OD_{560} in each well using an enzyme marker. PBS was used as a negative control and PBS containing 1% Triton X-100 was used as a positive control. Hemolysis was calculated by the following equation.

$$\text{Percentage hemolysis (\%)} = (\text{sample absorbance} - \text{negative control absorbance})/(\text{positive control absorbance} - \text{negative control absorbance}) \times 100.$$

2.10. Statistical analysis

For all experiments, data were presented as the mean ± SD (standard deviation). Data analysis was performed by using GraphPad Prism 8 and statistically analyzed using paired *t* tests and a one-way ANOVA. The difference was considered significant when $p < 0.05$ ($^{\#/*}$).

3 Results and discussion

3.1 Preparation of F(AM)-based copolymer and NPs

The amphiphilic copolymer F(AM) was synthesized by the PET-RAFT polymerization technique and then assembled to produce drug-loaded NPs (Fig. 1(a)). The hydrophobic fraction PF was synthesized using F as monomers, DDMAT as the CTA, and $Ir(ppy)_3$ as the photoinitiator. Then, the resulting PF was further used as a micro-RAFT reagent, using A_{Boc} and M_{OAc} together as monomers to synthesize $F(A_{Boc}M_{OAc})$ (Scheme S1, ESI†).^{1}H NMR spectroscopy and GPC analysis showed that the molecular weights of PF and $F(A_{Boc}M_{OAc})$ were ~7069 (M_w/M_n = 1.34) and ~11451 g mol^{-1} (M_w/M_n = 1.89), respectively (Fig. S1–S3, and Table S1, ESI†). The polymerization degrees of PF, the poly(β-*N*-acryloyl-α-Boc-D-aminoalanine) chain segment, and the poly(2-(2′,3′,4′,6′-tetra-*O*-acetyl-α-D-mannosyloxy) ethyl acrylate) chain segment were 28, 12, and 10, respectively (Fig. S4, ESI†). The final polymer F(AM) was obtained by deprotection and confirmed by ^{1}H NMR analysis (Fig. S5, ESI†). Then, F(AM) was self-assembled to form NPs in a water/DMSO (9/1, v/v) solvent system (Fig. 1(a)). TEM images showed that the F(AM) NPs exhibited a spherical morphology and had a uniform size (Fig. 1(b)). The average diameter of the F(AM) NPs was 220 nm (Fig. 1(c)). These results indicate that the F(AM) NPs were successfully constructed.

3.2 Cellular targeting and intracellular bacterial targeting

The F(AM) DDS was designed to deliver drugs on-site at the location of intracellular pathogens.[44] Therefore, the specific functions of F(AM) NPs for targeting host cells and intracellular bacteria were investigated. First, the specific targeting ability of

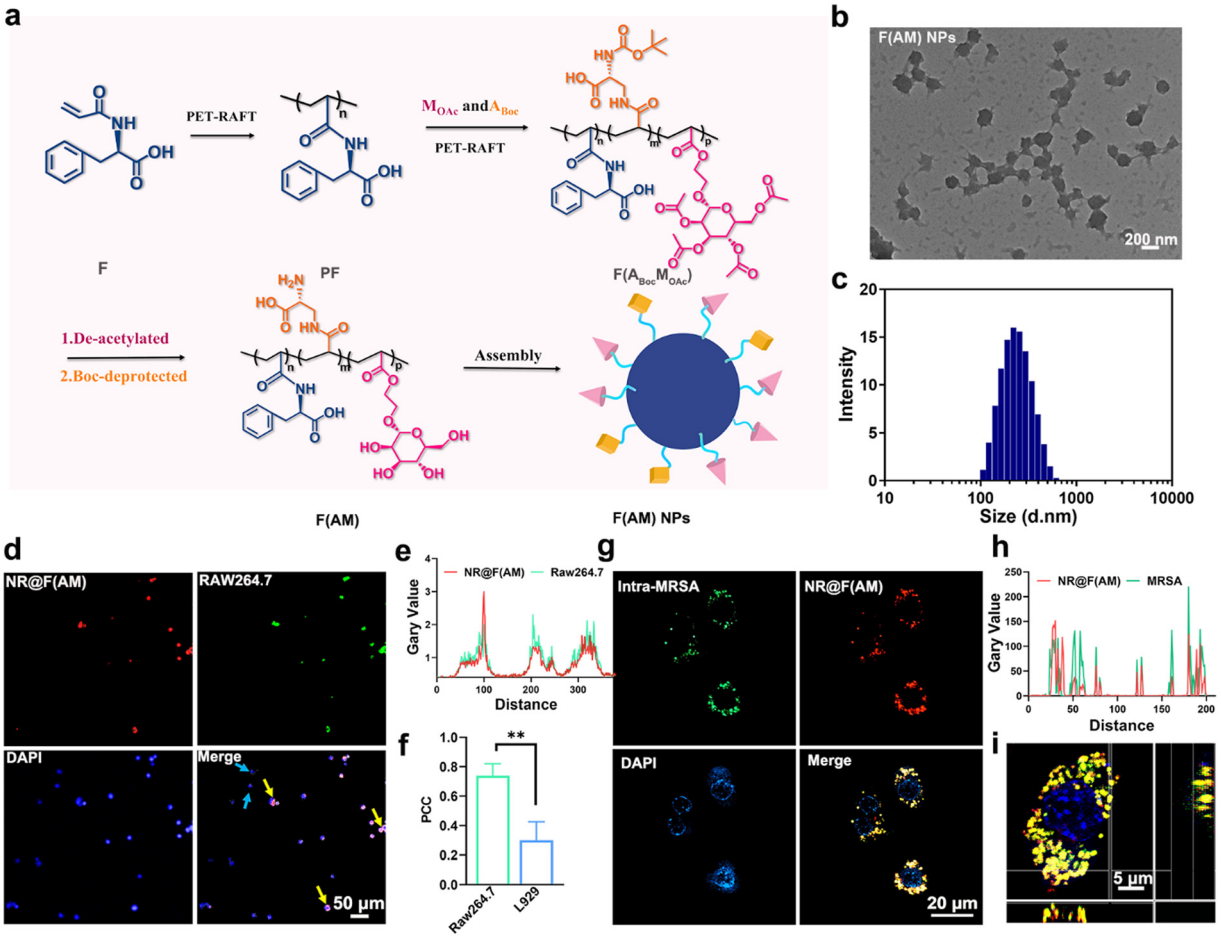

Fig. 1 (a) Construction process of F(AM) NPs. (b) TEM images and (c) DLS of F(AM) NPs. (d) Confocal images of NR@F(AM) NPs (10 μg mL^{-1} NR) after co-incubation with RAW264.7 macrophages and L929 fibroblasts for 1 h. (e) Co-localization fluorescence intensity distribution between NR@F(AM) NPs and RAW264.7 macrophages, which was analyzed using Image J software. (f) PCC was calculated using Image J software, $n = 6$, (** $p < 0.01$). (g) Confocal images of intracellular FITC-MRSA after incubation with NR@F(AM) NPs for 24 h. (h) Co-localization between NR@F(AM) NPs, and FITC-MRSA fluorescence intensity distribution. (i) 3D confocal images of RAW264.7 macrophages infected with FITC-MRSA after incubation with NR@F(AM) NPs.

F(AM) NPs for professional phagocytes, RAW264.7 macrophages, was investigated. NR@F(AM) NPs with red fluorescence were added to a mixed cell system containing calcein (AM)-labeled RAW264.7 macrophages (green fluorescence) and L929 fibroblasts cells. After 1 h of incubation, it was found that NR@F(AM) NPs bound more readily to RAW264.7 macrophages (yellow arrows), than L929 fibroblasts (blue arrows) (Fig. 1(d)). The Pearson correlation coefficient (PCC) of the co-localization between RAW264.7 macrophages and NR@F(AM) NPs was up to 0.739, significantly higher than that between L929 fibroblasts and NR@F(AM) NPs (0.300, Fig. 1(e)–(f), Fig. S6, ESI†). This implied that F(AM) NPs have a good macrophage-specific targeting ability. Subsequently, the intracellular bacterial targeting ability of F(AM) NPs was investigated. Intracellular bacteria-infected RAW264.7 macrophages were obtained using FITC-labeled MRSA and then co-incubated with NR@F(AM) NPs. As shown in Fig. 1(g), FITC-MRSA successfully infects RAW264.7 macrophages and is located in the cytoplasm. Importantly, the red fluorescence of the NR@F(AM) NPs matched well with the green fluorescence of the intracellular MRSA, exhibiting a bright yellow fluorescence in a merged image (Fig. 1(h)). The 3D confocal image with stereospecific visualization further confirmed that NR@F(AM) NPs perfectly targeted FITC-MRSA (Fig. 1(i)). The above results indicated that the constructed F(AM) NPs have excellent host cell and intracellular bacteria-specific targeting ability, which is an important foundation for on-site drug delivery.

3.3 Extracellular antibacterial evaluation and characterization of DDS

Van and Cur were selected drugs for encapsulation in the F(AM) NPs. Their extracellular bactericidal properties were systematically studied. Firstly, the synergistic bactericidal properties of the free drugs were investigated. MICs of Van and Cur were determined to be 1 μg mL^{-1} and 400 μg mL^{-1}, respectively (Fig. S7, ESI†). Cur showed a larger MIC value than Van. This is mainly because Cur disturbs and further damages cell membranes, resulting in bacterial death.[48] Van has a triple bactericidal mechanism, which includes inhibiting bacterial cell wall synthesis, altering bacterial cell membrane permeability, and

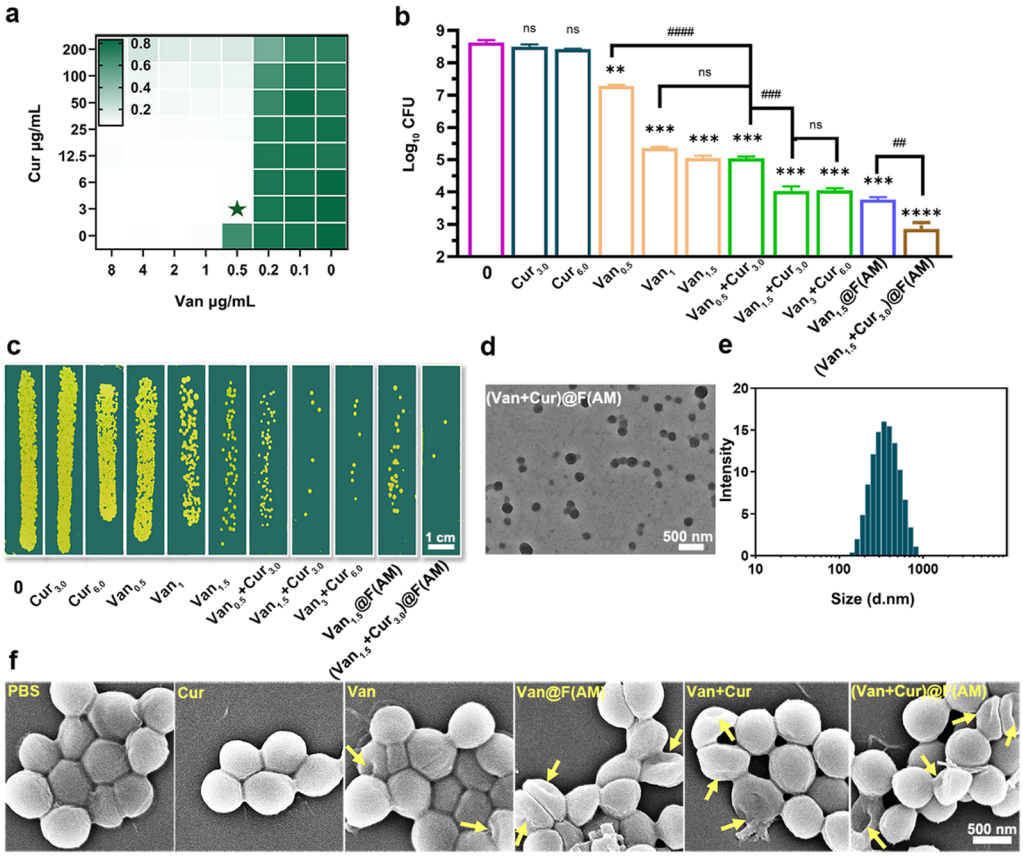

Fig. 2 Extracellular antibacterial evaluation. (a) Checkerboard dilution assays to evaluate the synergistic effect of Van and Cur. (b) CFU counting of extracellular MRSA with treatment of the free drugs. (c) Photographs of extracellular MRSA treated under different conditions. CFUs were counted using the drop plate method, $n = 3$. (d) TEM and (e) DLS of ($Van_{1.5}$ + $Cur_{3.0}$)@F(AM) NPs. (f) SEM images of bacteria treated under different conditions. Yellow arrows indicate defects in bacterial cell walls and membranes caused by antibiotics. $^{\#\#}/^{**}p < 0.01$, $^{\#\#\#}/^{***}p < 0.001$, $^{\#\#\#\#}/^{****}p < 0.0001$, and ns $p > 0.05$.

preventing RNA synthesis in the bacterial cytoplasm.[49,50] Interestingly, when 0.5 μg mL^{-1} of Van was combined with 3.0 μg mL^{-1} of Cur (denoted by ($Van_{0.5}$ + $Cur_{3.0}$)), the bacteriostatic efficiency was very much improved. The FICI was 0.507 (Fig. 2(a)), suggesting a synergistic bacteriostatic effect of the combination of Van and Cur. Furthermore, the quantitative antibacterial efficiency was evaluated by a colony count method. The bacterial colony count in the group of ($Van_{0.5}$ + $Cur_{3.0}$) was 5.1-Log_{10} CFU, which was reduced by 2.8-Log_{10} CFU compared to that in the group of $Van_{0.5}$ (0.5 μg mL^{-1}, Fig. 2(b) and (c)). These results implied that the combination of Van and Cur notably reinforced the bacteriostatic efficiency. This was mainly due to the fact that Cur increased the permeability of bacterial cell membranes, which enhanced the bactericidal mechanism of Van, and in particular, reinforced the inhibition of RNA synthesis in the bacterial cytoplasm by Van. Subsequently, the bactericidal performance of Van at a concentration of 1.5 × MIC (namely 1.5 μg mL^{-1}) was further investigated.[51] When $Van_{1.5}$ was used alone, its CFU count was 5.13 Log_{10} CFU, which approximated that of ($Van_{0.5}$ + $Cur_{3.0}$). Significantly, the CFU count of $Van_{1.5}$ could further decrease by 1.2-Log_{10} CFU in the presence of $Cur_{3.0}$. Upon further increasing the concentrations of Van and Cur, the combined ($Van_{3.0}$ + $Cur_{6.0}$) showed comparable antibacterial performance to ($Van_{1.5}$ + $Cur_{3.0}$), indicating the platform stage of the combined pharmacotherapy of Van and Cur. Therefore, based on the above results, we chose ($Van_{1.5}$ + $Cur_{3.0}$) as the final cargo to pack into F(AM) NPs. The assembly conditions, including drug proportion, solution proportion, and assembly speed were carefully controlled to obtain the final NPs, which were denoted by ($Van_{1.5}$ + $Cur_{3.0}$)@F(AM) NPs. After loading, the DLC of Van and Cur in the NPs was calculated to be ~13.5 wt% and ~23.2 wt%, respectively. The final content ratio of Van to Cur was about 1.5 : 3 (Fig. S8, S9, and Table S2, ESI†), suggesting that Van and Cur were successfully encapsulated into F(AM) NPs at a preset dose. Drug release results indicated that Van and Cur in the (Van + Cur)@F(AM) NPs were released in uniform and long-term patterns. Approximately 30% of Van or Cur was released at 72 h (Fig. S10, ESI†). Their similar release behaviors were mainly due to the π–π stacking interaction between Van and Cur.[52] This long-term, sustainable and stable multi-drug release is essential for the long-term inhibition of intracellular bacterial growth.[53,54] In addition, TEM images showed that ($Van_{1.5}$ + $Cur_{3.0}$)@F(AM) NPs were homogeneous spherical particles with an average

diameter of 357 nm (Fig. 2(d) and (e)), and their particle size and polydispersity index (PDI) did not change obviously over 1 month (Fig. S11, ESI†). The zeta potential of the ($Van_{1.5}$ + $Cur_{3.0}$)@F(AM) NPs was determined to be −41.4 mV (Fig. S12, ESI†). Additionally, $Van_{1.5}$@F(AM) NPs were used as a control, which was constructed and fully characterized (Fig. S13, ESI†).

Immediately after, the antibacterial properties of the drugs in the F(AM) NPs were investigated. Interestingly, $Van_{1.5}$@F(AM) NPs showed a 1.4-Log_{10} CFU reduction in bacterial colony count compared to $Van_{1.5}$ (Fig. 2(b)). This meant that F(AM) NPs possessing bacterial targeting properties could augment the bactericidal effect of Van. In other words, $Van_{1.5}$@F(AM) NPs that effectively killed bacteria might not only rely on the Van released from F(AM) NPs because of its long-periodic and slow release. It was noted that the D-alanine terminal in F(AM) NPs can tightly insert into the bacterial cell wall and interface the biosynthesis of peptidoglycan of the bacteria. Therefore, the F(AM) NPs would sensitize the bactericidal effect of Van, and alternatively, $Van_{1.5}$@F(AM) NPs could be internalized in the process of bacterial proliferation. In terms of this, $Van_{1.5}$@F(AM) NPs showed higher bactericidal efficacy than the naked Van. Moreover, the bacterial colony count of the ($Van_{1.5}$ + $Cur_{3.0}$)@F(AM) NPs was further reduced by 0.9 Log_{10} CFU compared with that of $Van_{1.5}$@F(AM) NPs, indicating that the dual drug encapsulated in the F(AM) NPs could effectively play a synergistic bactericidal role and enhance the elimination effect of MRSA. SEM images (Fig. 2(f)) showed that the bacteria in the PBS group as well as the Cur group had normal shapes, clear borders, and good membrane integrity. In contrast, severe collapse of bacterial cell membranes could be seen when the bacteria were treated with various NPs. In particular, bacterial content flowed out after treatment with ($Van_{1.5}$ + $Cur_{3.0}$)@F(AM) NPs. The above results again indicated that the F(AM)-based DDS was able to effectively exhibit a dual-drug synergistic bactericidal effect, providing a basis for supporting intracellular synergistic bactericidal activity in the host.

3.4 Intracellular antibacterial evaluation

Given the outstanding extracellular antibacterial properties of the ($Van_{1.5}$ + $Cur_{3.0}$)@F(AM) NPs, we further investigated their intracellular bactericidal effect in an MRSA-infected RAW264.7 macrophage model. As a control group, the naked F(AM) NPs and $Cur_{3.0}$ had no bactericidal effect (Fig. S14, ESI†). The free $Van_{1.5}$ showed inhibition of intracellular bacteria at the first 12 h (4.15 Log_{10} CFU, Fig. 3(a)). As the incubation time was extended to 24 h and 48 h, the free $Van_{1.5}$, however, lost its ability of intracellular bacterial inhibition. The counts of the

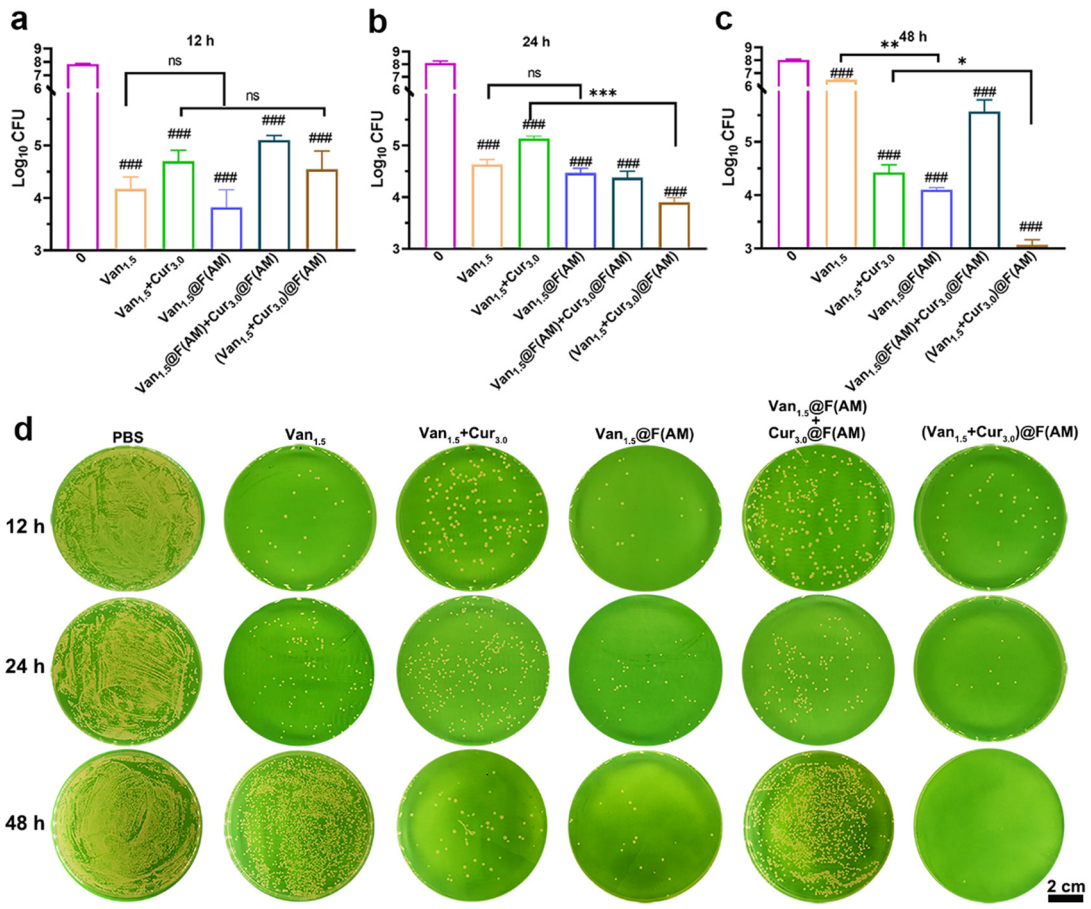

Fig. 3 Intracellular antibacterial evaluation. CFU count of intracellular MRSA at (a) 12 h, (b) 24 h, and (c) 48 h after different group treatments. (d) CFU photographs of intracellular MRSA. *$p < 0.05$, **$p < 0.01$, ###/***$p < 0.001$, and ns $p > 0.05$ respectively, $n = 3$.

treated bacteria gradually increased to 6.3 Log_{10} CFU (Fig. 3(b) and (c)). In addition, when the Van dose was increased at a gradient to 50 μg mL^{-1}, its bactericidal performance was not enhanced (4 Log_{10} CFU, Fig. S15, ESI†). This indicated that for free Van it was difficult to achieve long-term and effective bactericidal efficacy for intracellular infection. Primarily, the host cell membrane reduces the internalization of free Van. Additionally, the cellular efflux of the host cells shortens the intracellular residence time of the Van.[55] Consequently, free Van failed to control intracellular infections. Surprisingly, when Van was combined with Cur ($Van_{1.5}$ + $Cur_{3.0}$), it did not exhibit better antibacterial performance than free $Van_{1.5}$ (5 Log_{10} CFU) at 24 h (4.5 Log_{10} CFU) (Fig. 3(a) and (b)), suggesting this naked drug combination was ineffective against intracellular bacteria. This might be because the different internalization pathways and subcellular organelle distributions in the host cells attenuated the drug combination effect. But interestingly, by extending the incubation time to 48 h, ($Van_{1.5}$ + $Cur_{3.0}$) showed a more stable bactericidal efficacy than $Van_{1.5}$. It was reasonable that the intracellular accumulation of the two drugs reached equilibrium and subsequently exerted a certain combined bactericidal effect for long-term administration. Nevertheless, poor intracellular drug formulation and delayed drug combination result in the failed intracellular antibacterial performance of ($Van_{1.5}$ + $Cur_{3.0}$). The above results suggested that free drugs would be shielded by the host cell membrane, and that differences in the timing of internalization and intracellular spatial distribution severely reduced the synergistic effects of combined drugs.

The on-site drug delivery system was expected to solve this problem. First, $Van_{1.5}$@F(AM) NPs showed better intracellular MRSA inhibition compared with the free $Van_{1.5}$ (p = 0.0011). Especially, a 2.2 Log_{10} CFU reduction in the number of bacterial colonies could be found at 48 h treatment (Fig. 3(a)–(c)). This implied that the F(AM)-based DDS could break through the cell membrane barriers and fight against the cellular efflux of the host cells because of its intracellular bacterial targeting property, allowing Van to effectively exert a bactericidal performance. Moreover, the antibacterial performance of the ($Van_{1.5}$ + $Cur_{3.0}$) drug combination could be fully evoked *via* the robust F(AM)-based DDS. ($Van_{1.5}$ + $Cur_{3.0}$)@F(AM) NPs showed the lowest bacterial colony count compared to all other treatments. The ($Van_{1.5}$ + $Cur_{3.0}$)@F(AM) NPs showed a 2.2 Log_{10} CFU reduction in bacterial colonies at 24 h treatment compared to the ($Van_{1.5}$ + $Cur_{3.0}$) (Fig. 3(b)). Further extending treatment time to 48 h, the number of bacterial colonies in the group of ($Van_{1.5}$ + $Cur_{3.0}$)@F(AM) NPs was further significantly reduced by 1.6 Log_{10} CFU, while that was slightly decreased in the group of ($Van_{1.5}$ + $Cur_{3.0}$) (Fig. 3(c) and (d)). At the same time, ($Van_{1.5}$ + $Cur_{3.0}$)@F(AM) NPs also showed a better antibacterial effect than $Van_{1.5}$@F(AM) NPs, fully demonstrating the enduring bactericidal performance of (Van + Cur)@F(AM) NPs *via* its intracellular synergistic effect. To further shed light on this fact, $Van_{1.5}$@F(AM) NPs and $Cur_{3.0}$@F(AM) NPs were administered simultaneously to investigate the antibacterial performance. Though $Van_{1.5}$@F(AM) NPs + $Cur_{3.0}$@F(AM) NPs showed a slightly antibacterial effect at the first 24 h, they failed to control the proliferation of the intracellular bacteria at 48 h (Fig. 3(a)–(c)). The results suggested that when Van and Cur were encapsulated in the DDS separately, they would compete with each other during the processes of cell entry and intracellular bacterial targeting. Therefore, this independent encapsulation resulted in their different dosage at the location of the intracellular bacteria and ultimately attenuated the bactericidal effect.

Overall, the ($Van_{1.5}$ + $Cur_{3.0}$)@F(AM) NPs exhibited the best intracellular bacterial clearance. This excellent DDS, by delivering drugs on-site to the site of intracellular infection, enabled the synergistic bactericidal effect of the drug combination in the cells, resulting in long-term and high-efficient intracellular bacterial elimination.

3.5 Mechanism of the intracellular synergistic effect of the drug combination

Free drugs either in single or combined forms failed to kill intracellular bacteria because of their inherent limitations. As Fig. 4(a) illustrates, Van is a glycopeptide antibiotic that enters macrophages by endocytosis. Its accumulation is very slow and limited because of the efflux effect of the host cells.[33,56] Van that partially enters macrophages is mainly distributed in the subcellular organelle lysosomes.[57] Similarly, Cur is a natural antibacterial agent that enters cells mainly by rapid free diffusion, and it is mainly distributed in the subcellular organelle mitochondria.[58] As such, it is difficult for Van and Cur to exert the synergistic antibacterial effect due to the difference in their temporal and spatial distribution in the host cells (Fig. 4(a)). In contrast, the dual drug piggybacking on the F(AM)-based DDS has shown excellent performance in eliminating intracellular MRSA, mainly due to the intracellular synergistic effect of the drug combination of Van and Cur. The unified internalization of Van and Cur assisted by F(AM) NPs was the crucial first step for the whole intracellular journey. To clarify the internalization pathway, we systematically investigated the cellular uptake pathway of the F(AM)-based DDS. First, the RAW264.7 macrophages were pretreated at 4 °C and 37 °C to assess the energy dependence of the internalization process. After pretreatment at 4 °C, the cellular uptake of the FITC@F(AM) NPs was reduced by 81.5%, indicating their ATP-dependent internalization. The cellular uptake of the FITC@F(AM) NPs was further assessed in the presence of different internalization inhibitors. The inhibitors included sucrose, chlorpromazine (an inhibitor of lattice protein-mediated cellular endocytosis), methyl-β-cyclodextrin (β-CD, an inhibitor of niche protein-dependent endocytosis), and amiloride (an inhibitor of macrocytic drinking action).[59,60] Specifically, of all the internalization inhibitors treated for cellular uptake, the inhibition of microsphere uptake after amiloride treatment was the most pronounced, exhibiting a 33.3% reduction of internalization of FITC@F(AM) NPs. Accordingly, F(AM) NPs were mainly incorporated into cells through ATP-dependent macropinocytosis (Fig. 4(b) and (c)). The macropinocytosis process involves host cells encapsulating NPs in large vesicles, which then cause cell membrane folding

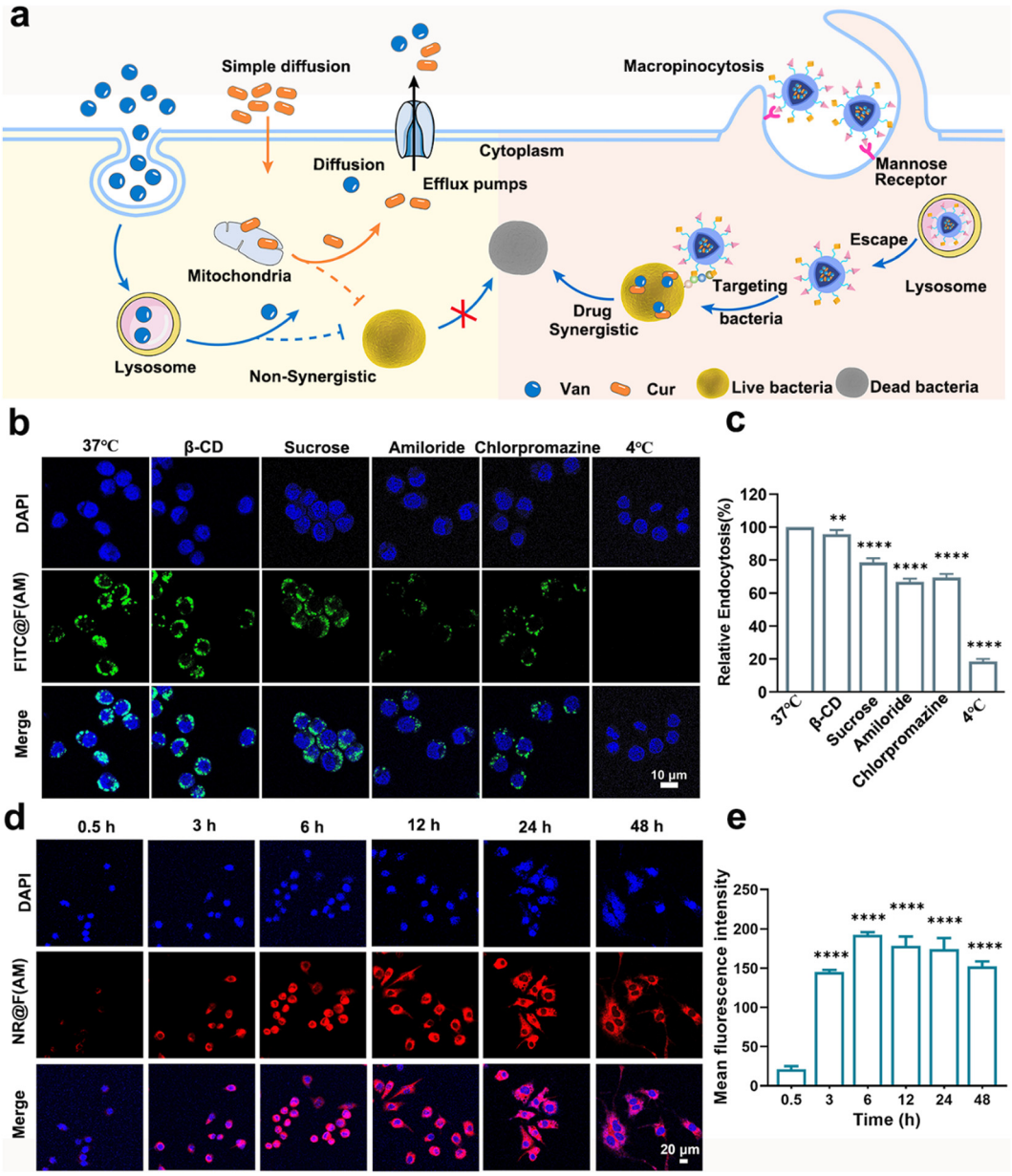

Fig. 4 (a) Schematic diagram of the mechanism of intracellular synergistic effects. (b) The cellular uptake of FITC@F(AM) NPs after pretreatment with different competitive inhibitors and (c) quantitative analysis of the relative uptake after pretreatment. (d) CLSM images of cellular uptake of NR@F(AM) NPs incubated with RAW264.7 macrophages for 0.5, 3, 6, 12, 24, and 48 h. (e) The corresponding MFI of the cellular uptake, which was calculated using Image J software. $^{**}p < 0.01$, $^{****}p < 0.0001$, $n = 6$.

through actin signaling to take up NPs.[61,62] Normally, NPs in the size range of 200–500 nm are internalized *via* micropinocytosis and favor the triggering of rapid cellular uptake of macrophages.[63] Subsequently, to demonstrate the role played by mannose in cellular uptake, FITC@F(AM) NPs were co-incubated with RAW264.7 macrophages that were pretreated by different concentrations of mannose. The confocal results showed that the green fluorescence signal was significantly dimmed by mannose pretreatment, and the statistical MFI showed a dose-dependent inhibition (Fig. S16, ESI†). The results showed that the entry of FITC@F(AM) NPs into macrophages was competitively blocked by mannose ligand receptor-mediated action due to the presence of mannose receptors on the surface of the macrophages.[64,65] Therefore, the F(AM)-based DDS entered cells *via* a mannose-mediated specific recognition and active energy-consuming macropinocytosis pathway.

Next, we investigated the intracellular accumulation of the F(AM) DDS by incubating NR@F(AM) NPs with RAW264.7 macrophages at different times (Fig. 4(d) and (e)). After 0.5 h of coincubation, the NR@F(AM) NPs were able to accumulate rapidly in the cells; extending the coincubation time could increase the cellular uptake of NR@F(AM) NPs, and NR@F(AM) NPs showed the strongest fluorescence at 6 h. Further increasing the coincubation time would slightly decrease the

fluorescence intensity. But up to 48 h, a high fluorescence intensity was still clearly observed (Fig. 4(d) and (e)). The results indicated that the F(AM)-based DDS could rapidly enter the cell and become enriched intracellularly for a long period. This might be the reason that ($Van_{1.5}$ + $Cur_{3.0}$)@F(AM) NPs exhibited long-term bactericidal performance. In addition, the ability of lysosomal escape is essential for F(AM) NPs to target intracellular bacteria.[66] Next, the colocalization between F(AM) NPs and lysosomes was investigated. Lysosomes were stained by Lyso-Tracker red with red fluorescence, and the PCC between the lysosome and intracellular FITC@F(AM) NPs was calculated (Fig. S17, ESI†). It could be seen that the PCC decreased from 0.9245 to 0.6238 when the incubation time was increased from 3 h to 12 h. Meanwhile, the accumulation of F(AM) NPs in the host cells increased as illustrated in Fig. 4(d) and (e). These results strongly implied that FITC@F(AM) NPs were able to escape from the lysosome to the cytoplasm. This was likely due to the exposed amino groups on the F(AM) NPs facilitating the transport of NPs from the lysosome to the cytoplasm.[67] In summary, the F(AM)-based DDS rapidly entered macrophages

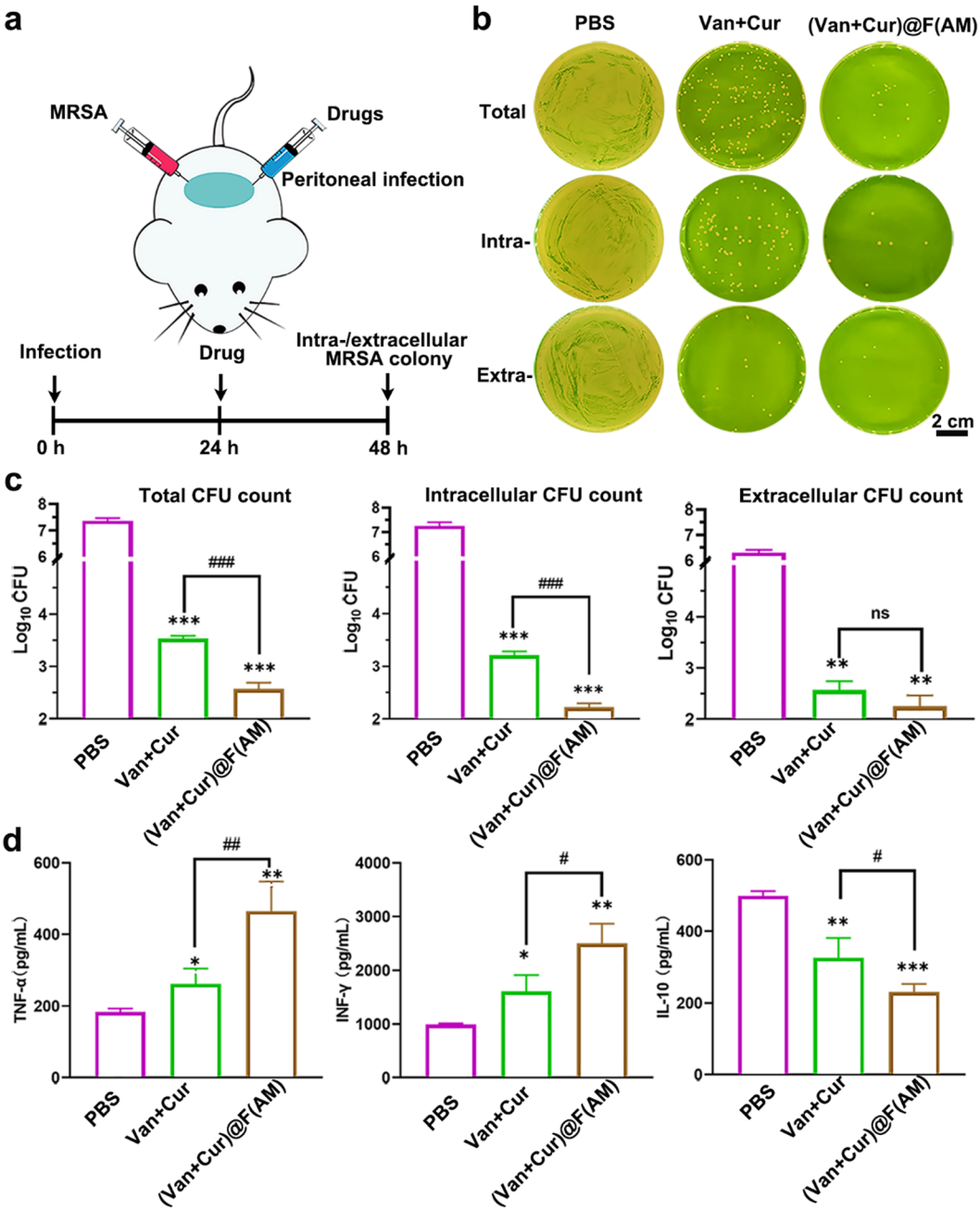

Fig. 5 (a) Schematic diagram of the mouse intraperitoneal infection model. Van (10 mg kg^{-1}) and Cur (20 mg kg^{-1}) were used for the antibacterial assays. (b) Photographs and (c) CFUs in the total, intracellular and extracellular fractions determined after the different group treatments for 24 h. (d) IL-10, TNF-α, and INF-γ expression in the serum were detected by ELISA kits. $^{\#/*}p < 0.05$, $^{\#\#/**}p < 0.01$, $^{\#\#\#/***}p < 0.001$, and ns $p > 0.05$, $n = 3$.

through mannose receptor-mediated micropinocytosis, and then F(AM) NPs were able to escape from lysosomes, and ultimately targeted intracellular bacteria to precisely release Van and Cur, achieving effective intracellular bacterial clearance through the long-term intracellular synergistic effect of this drug combination. Therefore, F(AM)-based DDS had a high potential for intracellular bacterial clearance.

3.6 *In vivo* antibacterial evaluation (peritoneal model)

The biosafety of (Van + Cur)@F(AM) NPs was then evaluated. The cytotoxicity of the F(AM) polymer and (Van + Cur)@F(AM) NPs toward RAW264.7 macrophages and L929 fibroblasts was tested. The F(AM) polymer and (Van + Cur)@F(AM) NPs showed low cytotoxicity at wide-range dosages of ≤ 90 μg mL^{-1} (Fig. S18 and S19, ESI†), indicating their cytocompatibility. Furthermore, the hemolysis assay revealed that (Van + Cur)@F(AM) NPs had good hemocompatibility. Even at a high concentration of 800 μg mL^{-1}, only 1.8% hemolysis was observed. These results demonstrated that the F(AM)-based DDS could be safely applied for the treatment of intracellular bacterial infections. Then, the *in vivo* antibacterial effect of (Van + Cur)@F(AM) NPs was further investigated using a mouse abdominal infection model (Fig. 5(a)). Therapeutic doses of Van and Cur in (Van + Cur)@F(AM) NPs were set at 10 mg kg^{-1} and 20 mg kg^{-1}, respectively. PBS, Van, Cur, (Van + Cur) and the naked F(AM) NPs were used as control groups (Fig. 5(b), (c) and Fig. S20, ESI†). Total, extracellular, and intracellular MRSA bacterial colony counts in the peritoneal fluid were determined after 24 h of treatment. For extracellular MRSA, (Van + Cur)@F(AM) NPs and (Van + Cur) showed comparable elimination efficiency (Fig. 5(b), (c) and Fig. S20, ESI†), which was higher than that of Van. This result was in agreement with the extracellular antibacterial evaluation. For intracellular MRSA, the (Van + Cur)@F(AM) NPs showed better antibacterial performance than (Van + Cur) and Van due to the excellent intracellular bacteria targeting ability of the F(AM)-based DDS. As such, for the total MRSA, (Van + Cur)@F(AM) NPs showed a better treatment effect (2.3 Log_{10} CFU) than (Van + Cur) (3.3 Log_{10} CFU) and Van (4.18 Log_{10} CFU). Comparatively, the naked NPs and Cur did not show significant treatment effects. These results indicated that the intracellular synergistic effect of the drug combination reinforced the intracellular bactericidal performance. Additionally, Cur can promote the immune function of the body.[68] Pro-inflammatory cytokine (IL-10, TNF-α, INF-γ) assay indicated that (Van + Cur)@F(AM) NPs treatment significantly reduced IL-10 levels but increased TNF-α and INF-γ levels (Fig. 5(d)). TNF-α and INF-γ are representative immune cytokines produced by M1 macrophages (M1 is associated with high antibacterial activity), and IL-10 is representative immune cytokines produced by M2 macrophages (M2, produces suppressive cytokines).[69–71] Thus, the above results suggested that (Van + Cur)@F(AM) NPs mobilized the body's immunity by affecting immune cytokines, allowing for further therapeutic efficacy against intracellular bacterial infections. Furthermore, H&E analysis (Fig. S21, ESI†) revealed that the lungs of mice in the PBS group showed tissue damage, such as significant heterogeneous expansion of the alveolar ducts. In contrast, (Van + Cur)@F(AM) NPs showed no significant difference in the H&E analysis compared with the healthy group. Based on these results, the proposed (Van + Cur)@F(AM) NPs exhibited excellent ability to eliminate intracellular bacteria through the synergistic effects of intracellular drug combinations and *in vivo* immune response.

4 Conclusions

In summary, robust (Van + Cur)@F(AM) NPs were proposed to achieve superior intracellular bacterial elimination *via* the intracellular synergistic effect of the drug combination. (Van + Cur)@F(AM) NPs effectively broke through the multiple physiological barriers of the host cell and enabled efficient accumulation of the drugs at bacterial residency sites through on-site drug delivery. Van and Cur in (Van + Cur)@F(AM) NPs were released in uniform and long-term patterns, reinforcing their durable synergistic bactericidal effects. Additionally, (Van + Cur)@F(AM) NPs were capable of inducing an *in vivo* immune response, facilitating intracellular antibacterial performance. Thus, (Van + Cur)@F(AM) NPs showed optimal intracellular MRSA elimination effects both *in vitro* and *in vivo*. Overall, this study provides a promising candidate for eliminating intracellular bacteria through intracellular multidrug synergy.

Author contributions

Guofeng Li and Xing Wang: design and interpretation of the study, writing – reviewing, and editing, supervision, project administration, funding acquisition; Dongdong Zhao: design of experiments, materials preparation and evaluation, animal experiment, data curation, writing – original draft preparation; Wenli Feng and Xiaoxu Kang: assistance of intracellular antibacterial evaluation; Fang Liu: assistance of *in vivo* antibacterial evaluation; Haofei Li: assistance of polymeric synthesis; Weitao Zheng: assistance of data analysis.

Conflicts of interest

The authors declare that they have no known competing financial interests or personal relationships that could have appeared to influence the work reported in this paper.

Acknowledgements

This work was supported by the National Natural Science Foundation of China (22275013, 52273118, and 22005020).

References

1 W. Feng, M. Chittò, T. F. Moriarty, G. Li and X. Wang, *Macromol. Biosci.*, 2022, 2200311.
2 S. Y. Tong, J. S. Davis, E. Eichenberger, T. L. Holland and V. G. Fowler Jr, *Clin. Microbiol. Rev.*, 2015, **28**, 603–661.

3 X. Liu, F. Liu, S. Ding, J. Shen and K. Zhu, *Adv. Sci.*, 2020, **7**, 1900840.
4 S. Trouillet-Assant, L. Lelièvre, P. Martins-Simões, L. Gonzaga, J. Tasse, F. Valour, J. P. Rasigade, F. Vandenesch, R. L. Muniz Guedes and A. T. Ribeiro de Vasconcelos, *Cell. Microbiol.*, 2016, **18**, 1405–1414.
5 C. Guarch-Pérez, M. Riool and S. A. Zaat, *Eur. Cells Mater.*, 2021, **41**, 334–374.
6 J.-L. Mège, V. Mehraj and C. Capo, *Curr. Opin. Infect. Dis.*, 2011, **24**, 230–234.
7 M. Fraunholz and B. Sinha, *Front. Cell. Infect. Microbiol.*, 2012, **2**, 43.
8 J. H. Zheng, V. H. Nguyen, S.-N. Jiang, S.-H. Park, W. Tan, S. H. Hong, M. G. Shin, I.-J. Chung, Y. Hong and H.-S. Bom, *Sci. Transl. Med.*, 2017, **9**, eaak9537.
9 C. Garzoni and W. L. Kelley, *Trends Microbiol.*, 2009, **17**, 59–65.
10 X. Wang, X. Wang, D. Teng, R. Mao, Y. Hao, N. Yang, Z. Li and J. Wang, *Sci. Rep.*, 2018, **8**, 1–15.
11 N. Abed and P. Couvreur, *Int. J. Antimicrob. Agents*, 2014, **43**, 485–496.
12 M. A. Fischbach, *Curr. Opin. Microbiol.*, 2011, **14**, 519–523.
13 G. Cottarel and J. Wierzbowski, *Trends Biotechnol.*, 2007, **25**, 547–555.
14 D. Xu, J. Wen, W. Fu, T. Gu and I. Raad, *World J. Microbiol. Biotechnol.*, 2012, **28**, 1641–1646.
15 L. Fan, B. Jin, S. Zhang, C. Song and Q. Li, *Nanoscale*, 2016, **8**, 12553–12559.
16 M. Paul, A. Lador, S. Grozinsky-Glasberg and L. Leibovici, *Cochrane Database Syst. Rev.*, 2014, **1**, CD003344.
17 M. Bassetti, E. Repetto, E. Righi, S. Boni, M. Diverio, M. Molinari, M. Mussap, S. Artioli, F. Ansaldi and P. Durando, *J. Antimicrob. Chemother.*, 2008, **61**, 417–420.
18 P. D. Tamma, S. E. Cosgrove and L. L. Maragakis, *Clin. Microbiol. Rev.*, 2012, **25**, 450–470.
19 L. Ejim, M. A. Farha, S. B. Falconer, J. Wildenhain, B. K. Coombes, M. Tyers, E. D. Brown and G. D. Wright, *Nat. Chem. Biol.*, 2011, **7**, 348–350.
20 E. K. Schneider, F. Reyes-Ortega, T. Velkov and J. Li, *Essays Biochem.*, 2017, **61**, 115–125.
21 H. E. Elphick and A. Scott, *Cochrane Database Syst. Rev.*, 2016, **12**, CD002007.
22 S. M. Lehar, T. Pillow, M. Xu, L. Staben, K. K. Kajihara, R. Vandlen, L. DePalatis, H. Raab, W. L. Hazenbos and J. Hiroshi Morisaki, *Nature*, 2015, **527**, 323–328.
23 M. Cruciani, G. Gatti, L. Lazzarini, G. Furlan, G. Broccali, M. Malena, C. Franchini and E. Concia, *J. Antimicrob. Chemother.*, 1996, **38**, 865–869.
24 C. Lamer, V. De Beco, P. Soler, S. Calvat, J. Fagon, M. Dombret, R. Farinotti, J. Chastre and C. Gibert, *Antimicrob. Agents Chemother.*, 1993, **37**, 281–286.
25 M. H. Kollef, *Clin. Infect. Dis.*, 2007, **45**, S191–S195.
26 S. Thangamani, W. Younis and M. N. Seleem, *PLoS One*, 2015, **10**, e0133877.
27 M. Chu, M.-B. Zhang, Y.-C. Liu, J.-R. Kang, Z.-Y. Chu, K.-L. Yin, L.-Y. Ding, R. Ding, R.-X. Xiao and Y.-N. Yin, *Sci. Rep.*, 2016, **6**, 1–9.
28 P. Agarwala, T. Bera and D. K. Sasmal, *ChemPhysChem*, 2022, **23**, e202200.
29 S.-Y. Teow, K. Liew, S. A. Ali, A. S.-B. Khoo and S.-C. Peh, *J. Trop. Med.*, 2016, **2016**, 2853045.
30 S. Yadav, A. K. Singh, A. K. Agrahari, K. Sharma, A. S. Singh, M. K. Gupta, V. K. Tiwari and P. Prakash, *Sci. Rep.*, 2020, **10**, 1–22.
31 A. Memarzia, M. R. Khazdair, S. Behrouz, Z. Gholamnezhad, M. Jafarnezhad, S. Saadat and M. H. Boskabady, *BioFactors*, 2021, **47**, 311–350.
32 S. Carryn, H. Chanteux, C. Seral, M.-P. Mingeot-Leclercq, F. Van Bambeke and P. M. Tulkens, *Infect. Dis. Clin.*, 2003, **17**, 615–634.
33 P. M. Tulkens, *Eur. J. Clin. Microbiol. Infect. Dis.*, 1991, **10**, 100–106.
34 P. Anand, A. B. Kunnumakkara, R. A. Newman and B. B. Aggarwal, *Mol. Pharmaceutics*, 2007, **4**, 807–818.
35 M. Ye, Y. Zhao, Y. Wang, M. Zhao, N. Yodsanit, R. Xie, D. Andes and S. Gong, *Adv. Mater.*, 2021, **33**, 2006772.
36 J. Trousil, O. Pavliš, P. Kubíčková, M. Škorič, V. Marešová, E. Pavlova, K. D. Knudsen, Y.-S. Dai, M. Zimmerman and V. Dartois, *J. Controlled Release*, 2020, **321**, 312–323.
37 K. Chen, Y. Ling, X. Li, D. Chen, X. Wang and R. Sun, *J. Controlled Release*, 2017, **259**, e73.
38 J. Yang, C. Wen, C. Pan, H. Guo, W. Zhao, J. Zhang, Y. Zhu, Y. Zhang and L. Zhang, *J. Mater. Sci.*, 2019, **54**, 9718–9728.
39 K. Lu, Y. Qu, Y. Lin, L. Li, Y. Wu, Y. Zou, T. Chang, Y. Zhang, Q. Yu and H. Chen, *ACS Appl. Mater. Interfaces*, 2022, **14**, 2618–2628.
40 S. Obuobi, K. Julin, E. G. Fredheim, M. Johannessen and N. Škalko-Basnet, *J. Controlled Release*, 2020, **324**, 620–632.
41 Y. Yu, J. Li, Y. Zhang, Z. Ma, H. Sun, X. Wei, Y. Bai, Z. Wu and X. Zhang, *Biomaterials*, 2022, **280**, 121309.
42 W. Feng, G. Li, L. Tao, Y. Wei and X. Wang, *Colloids Surf., B*, 2021, **202**, 111687.
43 W. Feng, Z. Huang, X. Kang, D. Zhao, H. Li, G. Li, J. Xu and X. Wang, *Biomacromolecules*, 2021, **22**, 4871–4882.
44 W. Feng, G. Li, X. Kang, R. Wang, F. Liu, D. Zhao, H. Li, F. Bu, Y. Yu and T. F. Moriarty, *Adv. Mater.*, 2022, **34**, 2109789.
45 R. A. Fisher, B. Gollan and S. Helaine, *Nat. Rev. Microbiol.*, 2017, **15**, 453–464.
46 G. Li, W. Feng, N. Corrigan, C. Boyer, X. Wang and J. Xu, *Polym. Chem.*, 2018, **9**, 2733–2745.
47 A. Nafis, A. Kasrati, C. A. Jamali, L. Custódio, S. Vitalini, M. Iriti and L. Hassani, *Antibiotics*, 2020, **9**, 140.
48 P. Tyagi, M. Singh, H. Kumari, A. Kumari and K. Mukhopadhyay, *PLoS One*, 2015, **10**, e0121313.
49 D. Kahne, C. Leimkuhler, W. Lu and C. Walsh, *Chem. Rev.*, 2005, **105**, 425–448.
50 S. Boonyarattanakalin, J. Hu, S. A. Dykstra-Rummel, A. August and B. R. Peterson, *J. Am. Chem. Soc.*, 2007, **129**, 268–269.
51 B. Maron, J. Rolff, J. Friedman and Z. Hayouka, *Microbiol. Spectrum*, 2022, **10**, e00973-22.
52 F. Huang, X. Cai, X. Hou, Y. Zhang, J. Liu, L. Yang, Y. Liu and J. Liu, *Exploration*, 2022, **2**, 20210145.

53 M. Fan, J. Si, X. Xu, L. Chen, J. Chen, C. Yang, J. Zhu, L. Wu, J. Tian and X. Chen, *Carbohydr. Polym.*, 2021, **257**, 117636.
54 S. M. Hosseini, R. Abbasalipourkabir, F. A. Jalilian, S. S. Asl, A. Farmany, G. Roshanaei and M. R. Arabestani, *Antimicrob. Resist. Infect. Control.*, 2019, **8**, 1–12.
55 F. C. Tenover, *Am. J. Med.*, 2006, **119**, S3–S10.
56 F. Van Bambeke, S. Carryn, C. Seral, H. Chanteux, D. Tyteca, M.-P. Mingeot-Leclercq and P. M. Tulkens, *Antimicrob. Agents Chemother.*, 2004, **48**, 2853–2860.
57 M. Barcia-Macay, F. Mouaden, M.-P. Mingeot-Leclercq, P. M. Tulkens and F. Van Bambeke, *J. Antimicrob. Chemother.*, 2008, **61**, 1288–1294.
58 R. Singh, H. H. Tønnesen, S. Kristensen and K. Berg, *Photochem. Photobiol. Sci.*, 2013, **12**, 559–575.
59 Q. Cai, Y. Fei, H.-W. An, X.-X. Zhao, Y. Ma, Y. Cong, L. Hu, L.-L. Li and H. Wang, *ACS Appl. Mater. Interfaces*, 2018, **10**, 9197–9202.
60 N. D. Donahue, H. Acar and S. Wilhelm, *Adv. Drug Delivery Rev.*, 2019, **143**, 68–96.
61 S. D. Conner and S. L. Schmid, *Nature*, 2003, **422**, 37–44.
62 J. Mercer and A. Helenius, *Nat. Cell Biol.*, 2009, **11**, 510–520.
63 H. Yue, W. Wei, Z. Yue, P. Lv, L. Wang, G. Ma and Z. Su, *Eur. J. Pharm. Sci.*, 2010, **41**, 650–657.
64 Q. Zhou, N. Gong, D. Zhang, J. Li, X. Han, J. Dou, J. Huang, K. Zhu, P. Liang and X.-J. Liang, *ACS Nano*, 2021, **15**, 2920–2932.
65 H.-L. Jiang, M. L. Kang, J.-S. Quan, S. G. Kang, T. Akaike, H. S. Yoo and C.-S. Cho, *Biomaterials*, 2008, **29**, 1931–1939.
66 X. Li, A. Mohamed Khamis, C. Zhang and Z. Su, *Pharm. Res.*, 2022, 1–19.
67 S. Roy, D. Zhu, W. J. Parak and N. Feliu, *ACS Nano*, 2020, **14**, 8012–8023.
68 R. M. Srivastava, S. Singh, S. K. Dubey, K. Misra and A. Khar, *Int. Immunopharmacol.*, 2011, **11**, 331–341.
69 M. Benoit, B. Desnues and J.-L. Mege, *J. Immunol.*, 2008, **181**, 3733–3739.
70 Z. Wu, J. Bai, G. Ge, T. Wang, S. Feng, Q. Ma, X. Liang, W. Li, W. Zhang and Y. Xu, *Adv. Healthcare Mater.*, 2022, **11**, 2200298.
71 S. Gordon, *Nat. Rev. Immunol.*, 2003, **3**, 23–35.

